Impact of Barrier Layer Thickness on SST in the Central Tropical North Atlantic*

GREGORY R. FOLTZ

University of Washington/Joint Institute for the Study of the Atmosphere and Ocean, Seattle, Washington

MICHAEL J. MCPHADEN

NOAA/Pacific Marine Environmental Laboratory, Seattle, Washington

(Manuscript received 31 October 2007, in final form 8 July 2008)

ABSTRACT

Measurements from three long-term moored buoys are used to investigate the impact of barrier layer thickness (BLT) on the seasonal cycle of sea surface temperature (SST) in the central tropical North Atlantic Ocean. It is found that seasonal variations of the BLT exert a considerable influence on SST through their modulation of the vertical heat flux at the base of the mixed layer, estimated as the residual in the mixed layer heat balance. Cooling associated with this term is strongest when the barrier layer is thin and the vertical temperature gradient at the base of the mixed layer is strong. Conversely, thick barrier layers are associated with a significant reduction in the vertical temperature gradient at the base of the mixed layer, which suppresses the upward transfer of cooler water into the mixed layer. Forced ocean and coupled ocean–atmosphere models that do not properly simulate the barrier layer may have difficulty reproducing the observed seasonal cycle of SST in the tropical North Atlantic.

1. Introduction

Tropical North Atlantic sea surface temperature (SST) exerts a significant influence on the climates of the surrounding continents, mainly through its effects on the position of the rain-producing intertropical convergence zone (ITCZ) (Folland et al. 1986; Hastenrath and Greischar 1993; Giannini et al. 2003) and its impact on tropical cyclone formation and intensification (e.g., Shapiro and Goldenberg 1998; Goldenberg et al. 2001; Wang et al. 2006; Kossin and Vimont 2007; Saunders and Lea 2008). The dominant source of SST variability in the tropical North Atlantic is the seasonal cycle (Mitchell and Wallace 1992). A thorough knowledge of the causes of seasonal SST variability is important for understanding interannual climate variability, which is closely linked to the seasonal cycle (Hastenrath 1984; Nobre and Shukla 1996; Okajima et al. 2003).

Previous studies have shown that the seasonal cycle of SST in the tropical North Atlantic is driven primarily by changes in surface shortwave radiation and latent heat loss (Carton and Zhou 1997; DeWitt and Schneider 1999; Foltz et al. 2003; Yu et al. 2006). Foltz et al. (2003) conducted a detailed mixed layer heat budget analysis at three Pilot Research Moored Array in the Tropical Atlantic (PIRATA) mooring locations along 38°W in the central tropical North Atlantic. They found that seasonal variations of SST are explained reasonably well by the combination of the net surface heat flux and horizontal heat advection, but noted a residual in the heat balance of $\sim \pm 50$ W m^{-2} throughout most of the year at 15° and 12°N. They attributed the residual to a combination of limited data availability and vertical turbulent mixing at the base of the mixed layer.

The seasonal cycle of salinity in the tropical North Atlantic Ocean is influenced by strong river discharge, precipitation, and the southward subduction of high-salinity water from the subtropical North Atlantic (Muller-Karger et al. 1988; Blanke et al. 2002; Foltz and McPhaden 2008). These factors can lead to shallow salinity stratification within a deeper isothermal layer, resulting in a ''barrier layer'' between the base of the isothermal layer and the base of the mixed layer (Sprintall and Tomczak

* Pacific Marine Environmental Laboratory Contribution Number 3194 and Joint Institute for the Study of the Atmosphere and Ocean Contribution Number 1486.

Corresponding author address: Gregory R. Foltz, NOAA/PMEL, 7600 Sand Point Way NE, Seattle, WA 98115.
E-mail: gregory.foltz@noaa.gov

DOI: 10.1175/2008JCLI2308.1

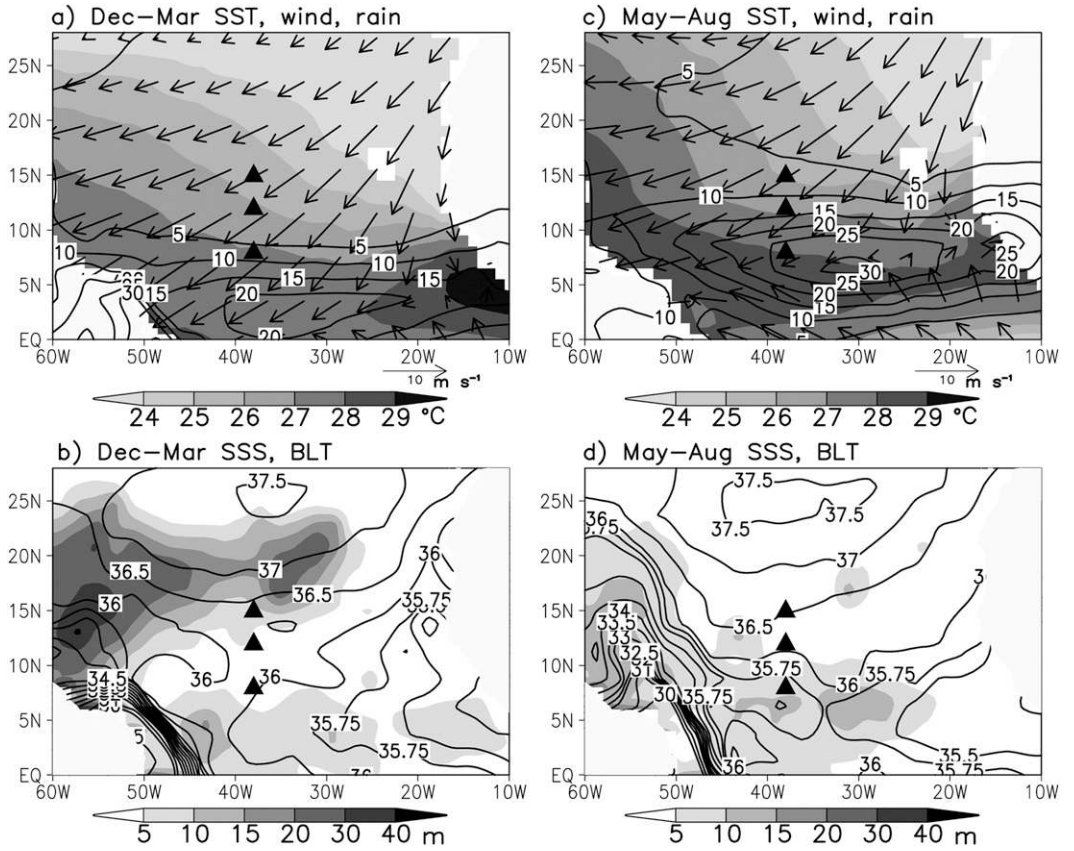

FIG. 1. Climatological (a) December–March and (c) May–August TMI SST (shaded), QuikSCAT wind velocity (vectors), and GPCP precipitation (contours, cm month^{-1}). Climatological barrier layer thickness (shaded) and surface salinity (contours, psu) for (b) December–March and for (d) May–August. Black triangles indicate locations of PIRATA moorings used in this study.

1992; Pailler et al. 1999; Foltz et al. 2004; Sato et al. 2006; de Boyer Montégut et al. 2007). The barrier layer is thickest on average in the northwestern tropical Atlantic and exhibits strong seasonal variability in the north-central basin (Sprintall and Tomczak 1992; Pailler et al. 1999; de Boyer Montégut et al. 2007; Mignot et al. 2007; Fig. 1).

In the tropical Pacific and Indian Oceans barrier layers affect SST by reducing the entrainment of cool thermocline water into the mixed layer (e.g., Vialard and Delecluse 1998; Maes et al. 2002; Masson et al. 2005). The impact of barrier layer thickness (BLT) on SST in the tropical Atlantic has received considerably less attention. Pailler et al. (1999) analyzed high vertical resolution measurements of salinity and temperature to show that high SSTs in the northwestern tropical Atlantic are often associated with low sea surface salinity (SSS) and thick barrier layers (>40 m). Masson and Delecluse (2001) used an ocean general circulation model to show that barrier layers north of the Amazon outflow can trap solar radiation and generate a temperature inversion at the base of the mixed layer. In their study, barrier layers and associated temperature inversions did not have a significant effect on SST. However, their model SST was restored toward climatology, potentially damping BLT-induced changes in SST. More recently, de Boyer Montégut et al. (2007) and Mignot et al. (2007) used in situ temperature and salinity profiles to show that the barrier layer in the northwestern tropical Atlantic is associated with temperature inversions of up to 0.5°C during boreal winter. They suggested that these conditions are maintained by the presence of subducted high-salinity subtropical thermocline waters combined with northward transport of fresher surface water and surface cooling. They also showed that vertical temperature inversions are much stronger in the northwestern tropical Atlantic in comparison to the central basin. The barrier layer may have important implications for modeling of tropical Atlantic climate. For example, Breugem et al. (2008) showed that coupled ocean–atmosphere models generally underestimate the BLT in the tropical North Atlantic,

contributing to significant cool SST biases in most models.

In this study we use measurements from three long-term moored buoys in the central tropical North Atlantic to investigate the role of barrier layer thickness in the seasonal cycle of SST. The present analysis complements the mixed layer heat budget analysis of Foltz et al. (2003), which was based on measurements from the same PIRATA moorings, and a recent study of Breugem et al. (2008), which is based on numerical model and ocean reanalysis output. The main advantage of the current study with respect to previous diagnostic efforts is its use of high temporal resolution subsurface temperature and salinity measurements, together with high quality surface flux measurements. This study also expands on the results of Foltz et al. (2003) through the use of longer data records and a detailed analysis of barrier layer effects on the mixed layer heat balance.

2. Datasets

We use data from three moored buoy sites of the Pilot Research Moored Array in the Tropical Atlantic (Servain et al. 1998) located at 15°, 12°, and 8°N along 38°W (Fig. 1). Measurements at these locations, begun in 1998 and continued through the present, include subsurface temperature and salinity, air temperature, relative humidity, wind velocity, shortwave radiation, and precipitation. From 1998 to present, ocean temperature was measured at 11 depths between 1 m (i.e., bulk SST) and 500 m, with 20-m spacing in the upper 140 m, while salinity was measured at 1, 20, 40, and 120 m. Since July 2005 at the 15°N location additional temperature measurements have been made at 10 and 13 m, additional salinity measurements at 10 and 60 m, and horizontal velocity at 10 m. Since December 2006 downward longwave radiation has been measured at the 15°N site. At all sites meteorological measurements are made at heights of 3–4 m above sea level.

We use daily-averaged data for the time period January 2000–August 2007. Data before 2000 are excluded owing to missing subsurface salinity measurements. The combination of instrument failure and vandalism limited the usable data record for this study to ~3 years at 12° and 8°N and ~6 years at 15°N (Fig. 2).

We also use measurements from several satellite and in situ sources. SST is available from the Tropical Rainfall Measuring Mission (TRMM) Microwave Imager (TMI) on a 0.5° × 0.5° × daily grid beginning December 1997. Surface wind velocity was obtained from the SeaWinds scatterometer onboard the Quick Scatterometer (QuikSCAT) satellite on a 0.25° × 0.25° × daily grid beginning July 1999. Monthly mean estimates of near-surface chlorophyll-*a* concentration were obtained from the Sea-Viewing Wide Field-of-View Sensor (SeaWiFS) onboard the *SeaStar* satellite. These data are available on a 0.08° × 0.08° grid for the time period 1997–present. We use monthly precipitation estimates from the Global Precipitation Climatology Project (GPCP) and daily air temperature estimates at a height of 2 m from the National Centers for Environmental Prediction/Department of Energy (NCEP/DOE) Reanalysis 2 (hereafter NCEP2) (Kanamitsu et al. 2002). Both of these datasets are available on a 2.5° × 2.5° grid for 1979–2006. We also use the monthly climatological sea surface salinity dataset of Foltz and McPhaden (2008), which is based on in situ vertical salinity profiles and surface salinity measurements and is available on a 2.5° × 2.5° grid, and the monthly net longwave radiation emission (LWR) climatology from the Comprehensive Ocean–Atmosphere Data Set (COADS) (da Silva et al. 1994), available on a 1° × 1° grid.

We obtained the monthly climatological BLT estimates of (de Boyer Montégut et al. 2007, hereafter BM07) on a 2° × 2° grid. These data are based on

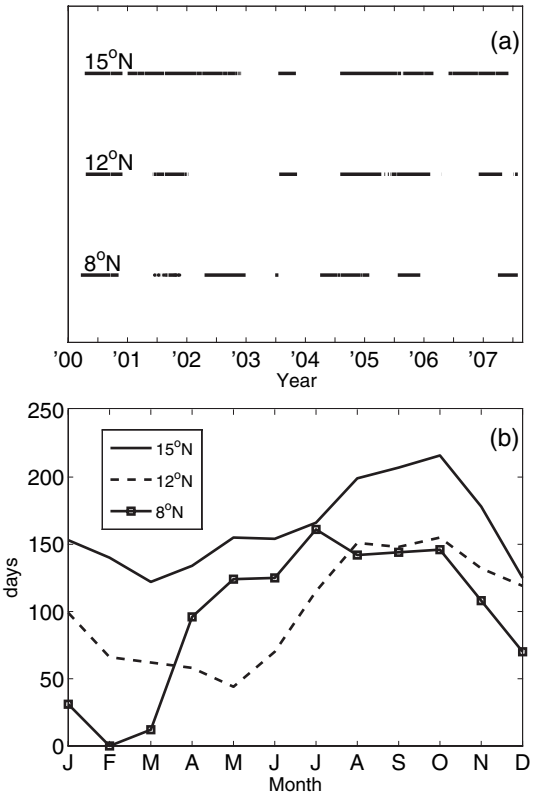

FIG. 2. (a) Availability of daily PIRATA measurements at (top) 15°N, 38°W; (middle) 12°N, 38°W; and (bottom) 8°N, 38°W (solid lines denote when all PIRATA variables are available). (b) Number of days in each climatological month for which all PIRATA variables are available.

individual temperature and salinity profiles from the World Ocean Database 2001 (WOD01). BM07 defined the BLT as the difference between the isothermal layer depth, calculated using the criterion of a 0.2°C decrease from a depth of 10 m, and the mixed layer depth, defined using the criterion for density equivalent to a 0.2°C decrease from a depth of 10 m (generally ~0.07 kg m^{-3} in the tropical North Atlantic). The criterion of the density equivalent of a 0.2°C temperature decrease from 10 m is generally small enough to capture the seasonal variations of MLD but large enough to avoid aliasing the effects of the diurnal cycle (BM07).

Three different estimates of horizontal mixed layer velocity are analyzed in this study. One calculates currents at an average depth of ~15 m using velocity estimates from surface drifters and ship drifts, together with satellite-based sea level and wind stress (Grodsky and Carton 2001, hereafter GC01). These data are available as a monthly climatology on a 2° latitude × 3° longitude grid. The second uses near-surface velocity from satellite-tracked drifting buoys and is available as a monthly mean climatology on a 1° × 1° grid (Lumpkin and Garzoli 2005, hereafter LG05). Finally, we obtained estimates of horizontal velocity averaged in the upper 30 m from the Ocean Surface Current Analysis–Real Time (OSCAR) (Bonjean and Lagerloef 2002). This method uses satellite sea level, wind stress, and SST, together with a diagnostic model, to calculate velocity on a 1° × 1° × 5 day grid for the time period 1993–present. The OSCAR product has the advantage of more complete spatial and temporal coverage than the ship drift and drifter-based climatologies because it uses satellite measurements, but has the disadvantage of not being constrained by direct velocity observations.

The QuikSCAT winds, GPCP precipitation, TMI SST, and SSS and BLT climatologies are used to describe the mean seasonal cycle in the tropical North Atlantic (Fig. 1). The PIRATA measurements, TMI SST, SeaWiFS chlorophyll-*a* concentration, NCEP2 air temperature, and GC01 mixed layer velocity climatology are used to assess the role of BLT in the mixed layer heat balances at the mooring locations. Finally, we use the OSCAR and LG05 velocity estimates and the COADS LWR estimates to assess uncertainties in horizontal mixed layer heat advection and LWR.

3. Methodology

a. Mixed layer heat equation

To address the causes of the seasonal cycle of SST at the mooring locations, we consider a simplified version of the mixed layer heat balance (e.g., Moisan and Niiler 1998):

$$\rho c_p h \frac{\partial T}{\partial t} = q_0 - \rho c_p h \mathbf{v} \cdot \nabla T + q_{-h} + \epsilon. \quad (1)$$

The terms in (1) represent, from left to right, mixed layer heat storage rate, surface heat flux corrected for the penetration of shortwave radiation through the base of the mixed layer, horizontal mixed layer heat advection, and the combination of entrainment and the vertical turbulent heat flux at the base of the mixed layer. Errors in the estimation of the terms in (1), and neglected physical processes, are represented by ϵ. Here h is the mixed layer depth and T and $\mathbf{v}$ are temperature and velocity, respectively, vertically averaged from the surface to a depth of $-h$. We estimate h and $\partial T/\partial t$ from subsurface temperature and salinity at the moorings, using the criterion of a 0.03 kg m^{-3} density increase from a depth of 10 m for h. Isothermal layer depth (ILD), used with h to estimate BLT, is computed using the temperature equivalent of a 0.03 kg m^{-3} density criterion (generally 0.1°C in the tropical North Atlantic).

Our choice of the 0.03 kg m^{-3} criterion is based mainly on the vertical resolution of salinity measurements at the moorings. At 12° and 8°N and for most of the data record at 15°N there are no salinity measurements between 40 and 120 m. We found that there are significant differences between the mooring-based MLD and estimates based on higher vertical resolution WOD01 when the MLD is >40 m (rms differences are up to 15 m when MLD is >40 m and <5 m when MLD is <40 m). A criterion of 0.03 kg m^{-3} gives a MLD that is <40 m throughout most of the year at each mooring location, minimizing uncertainties. The 0.03 kg m^{-3} criterion results in MLDs that are on average ~5 m shallower than the climatological estimates of Monterey and Levitus (1997), which are based on the criterion of a 0.125 kg m^{-3} criterion from the surface, and ~15 m shallower than the estimates of BM07, which are based on the criterion of a 0.07 kg m^{-3} criterion from a depth of 10 m. In addition, at 15° and 12°N the mooring-based barrier layer climatology is 5–10 m thicker than the BM07 climatology during boreal winter. The results of this study are not qualitatively changed for MLD (ILD) criteria ranging from 0.01–0.1 kg m^{-3} (0.05–0.3°C). A more quantitative comparison of MLDs for different density criteria is presented in sections 5 and 6.

The surface heat flux consists of latent and sensible heat loss, absorbed shortwave radiation, and net longwave radiation emission. Latent and sensible heat fluxes are estimated from version 3.0 of the Coupled Ocean–Atmosphere Response Experiment (COARE) bulk flux algorithm (Fairall et al. 2003) with buoy estimates of SST, air temperature, relative humidity, and wind speed. Due to possible low frequency drifts in air temperature during

some deployments at 15°N, we have replaced the buoy air temperature with NCEP2 air temperature before computation of the turbulent heat fluxes at this site. The results of Jiang et al. (2005) indicate that, in general, errors in latent heat flux associated with the substitution of NCEP2 air temperature for Tropical Atmosphere Ocean buoy air temperature are negligible ($\sim$1 W m^{-2}).

Surface shortwave radiation (SWR) is available directly from the moorings, assuming an albedo of 6%. Following Morel and Antoine (1994) and Sweeney et al. (2005), we model the amount of SWR penetrating the mixed layer as $q_{\rm pen} = 0.47q_{\rm sfc}(V_1e^{-h/d_1} + V_2e^{-h/d_2})$, where $q_{\rm sfc}$ is the surface shortwave radiation, d_1 and d_2 are the e-folding depths of the long visible (d_1) and short visible and ultraviolet (d_2) wavelengths, and h is the depth of the mixed layer in meters. The parameters V_1, V_2, d_1, and d_2 are estimated using SeaWiFS chlorophyll-a concentration following Sweeney et al. (2005). Net longwave radiation emission (LWR) is estimated from the Clark et al. (1974) bulk formula following the methodology of Foltz and McPhaden (2005). In this study we use the convention that surface heat fluxes are positive when they tend to heat the mixed layer.

Vertically averaged mixed layer velocity is estimated using the GC01 monthly climatology repeated for each year and interpolated to a daily resolution. The daily velocity estimates are then multiplied by daily TMI SST gradients, calculated as centered differences over a distance of 4°, in order to estimate horizontal mixed layer heat advection. The buoy and satellite SSTs agree reasonably well for the time period we consider. RMS differences are 0.1°C at 15°N and 0.2°C at 12° and 8°N. Our estimates of horizontal heat advection do not include variations of mixed layer velocity on time scales less than one month. Results for other velocity data products and the potential impact of high-frequency velocity fluctuations on the seasonal cycle of horizontal heat advection are discussed in section 5.

We have neglected a term in (1) that is proportional to the horizontal divergence of the vertically averaged temperature–velocity covariance [see Eq. (A19) of Moisan and Niiler 1998]. We found that this term is insignificant in comparison to the other terms in (1), based on monthly mean data for 2000–04 from the Simple Ocean Data Assimilation (SODA) (Carton et al. 2000). The annual mean and monthly standard deviation of the covariance term in SODA are -0.8 ± 1.2 W m^{-2} at 15°N, 0.1 ± 1.2 W m^{-2} at 12°N, and -0.3 ± 1.0 W m^{-2} at 8°N. The weakness of this term in comparison to the other terms in the heat balance is consistent with the results of Swenson and Hansen (1999) in the equatorial Pacific. We are also unable to reliably estimate q_{-h} directly and therefore estimate this term as the difference between the observed mixed layer heat storage rate [first term in (1)] and the sum of the net surface heat flux and horizontal advection [first and second terms on the right-hand side of (1), respectively].

b. Error estimates

One of the largest sources of error in this study is the calculation of h and T from the coarse vertical resolution of the temperature and salinity sensors on the moorings. In principle, the error in h on a given day can be as large as the vertical resolution of the temperature and salinity sensors on the moorings, which is $\sim$20 m in the upper 40 m and 80 m between 40 and 120 m. Consider the case in which MLD is $<$40 m. If the probability distribution for these errors is uniform between -20 and 20 m, then theory suggests that the mean error in mixed layer depth would be zero with a standard deviation of $\pm$12 m. We tested this theory as in Foltz and McPhaden (2008) using 386 WOD01 CTDs in the tropical North Atlantic (5°–20°N, 30°–60°W), which have a higher vertical resolution than the moorings. The probability distribution is in reality not uniform but highly skewed toward small positive values. Based on the empirical probability distribution for the full range of daily MLD values, including those that exceed 40 m, the typical random error in mooring-estimated h is $\pm$6 m, and the mean h calculated using the vertical resolution of the moorings is 4 m shallower than the mean h calculated from the higher-resolution WOD01. Thus, in our computations we have added a 4-m offset to mooring-estimated MLDs to compensate for the mean error. Foltz et al. (2003) estimated similar biases based on typical values of the vertical temperature gradient in the thermocline in the tropical Atlantic. From sensitivity tests using WOD01 data, we also found a typical random error in isothermal layer depth of $\pm$4 m and a mean offset of 2 m, with mooring-based estimates lower. We have therefore added a 2-m offset to the mooring-estimated ILD. Errors in mixed layer temperature are $\pm$0.03°C, with mooring-based estimates lower on average by 0.02°C.

Uncertainties for the mixed layer heat storage rate are estimated using the combination of sampling errors in h and T and instrumental errors for PIRATA temperature sensors (all PIRATA instrumental uncertainties are available online at http://www.pmel.noaa.gov/tao/proj_over/sensors.shtml). Errors in daily-averaged mixed layer heat storage rate are typically $\sim \pm 40$ W m^{-2} and are dominated by sampling errors in T.

Errors in the estimation of horizontal mixed layer heat advection result from errors in horizontal satellite SST gradients, mixed layer velocity, and h. We estimate errors in daily-averaged satellite SST as the rms difference

between satellite and mooring SST and assume errors in both components of horizontal mixed layer velocity of ± 5 cm s^{-1}. Errors in h are estimated using the sampling errors discussed previously in this section. Uncertainties in mixed layer velocity and horizontal SST gradients dominate the errors in advection, leading to errors in daily-averaged advection of $\sim \pm 10$ W m^{-2}.

Errors in the surface turbulent heat flux terms are estimated using instrumental errors for air temperature, SST, wind speed, and relative humidity (0.2°C, 0.02°C, 0.3 m s^{-1}, and 2.7%, respectively), together with uncertainties associated with the estimation of latent heat flux (LHF) and sensible heat flux (SHF) from bulk algorithms (~12%; Fairall et al. 1996). Instrumental errors lead to uncertainties in daily LHF and SHF at each mooring location of $\sim \pm 15$ W m^{-2} and $\sim \pm 2$ W m^{-2}, respectively. Errors associated with the bulk algorithms give uncertainties in LHF and SHF of $\sim \pm 15$ W m^{-2} and $\sim \pm 1$ W m^{-2}, respectively. Total errors in daily LHF and SHF are $\sim \pm 20$ W m^{-2} and $\sim \pm 3$ W m^{-2}, respectively, where we have assumed that instrumental and bulk algorithm errors are uncorrelated in time.

Errors in LWR are the combination of instrumental errors (±1%) and errors in the LWR bulk flux algorithm. We estimate errors in the bulk algorithm as the monthly rms difference between our estimates of LWR, based on buoy measurements and the Clark et al. (1974) bulk algorithm, and COADS climatological LWR, which uses a different algorithm. We found rms differences of 2–3 W m^{-2} at each mooring location. Errors in absorbed SWR result from instrumental errors in surface SWR (±2%; Cronin and McPhaden 1997) and sampling errors in h. Errors due to surface SWR and h are typically ± 4 W m^{-2} each, giving total errors in absorbed SWR of $\sim \pm 6$ W m^{-2}.

To calculate errors for monthly averages of each parameter we first calculate the integral time scale for each month following Davis (1976). We found values of 2–3 days for each parameter averaged over the length of each data record. For simplicity we therefore use a value of 3 days in all calculations, giving ~10 degrees of freedom for each month. Averaging to monthly means therefore reduces random errors in daily data by a factor of ~3. Errors in monthly mean climatologies for each parameter are calculated from the monthly mean values as $N^{-1}\sqrt{\sum_{i=1}^{N} e_i^2}$, where N is the number of monthly values averaged for each climatological month and e_i is the error associated with each monthly value. In addition to the random errors described previously in this section, there may be significant annual mean and seasonal biases. A discussion of these uncertainties and their impact on our estimates of q_{-h} is provided in section 5.

4. Mixed layer heat balance

Before examining the impact of BLT on the mixed layer heat balance at the PIRATA mooring locations, we consider the large-scale climatological surface conditions in the tropical North Atlantic (Fig. 1). During boreal winter a zonal band of high SST (>27°C) and heavy rainfall (>15 cm mo^{-1}, associated with the ITCZ) is situated between the equator and 8°N. Thick barrier layers (>5 m) are present in the northwestern basin (west of 50°W) and in zonal bands centered near 20° and 5°N. In boreal summer the ITCZ is located farther north (5°–10°N) than in winter. The barrier layer disappears east of 50°W in the 10°–25°N latitude band and strengthens slightly in the vicinity of 5°–10°N. The decrease in BLT to the north results mainly from the combination of changes in the subsurface temperature and salinity structure and surface buoyancy forcing, while the increase in BLT between 5° and 10°N is likely due to a combination of increased precipitation and eastward advection of Amazon water (Sprintall and Tomczak 1992; Sato et al. 2006; Mignot et al. 2007).

Next we examine the mixed layer heat balances at the PIRATA mooring locations. The moorings are located to the southeast of the maximum BLT in the northwestern basin but still are found in a region of significant annual mean and strong seasonal variability of BLT (Fig. 1). Measurements from the northernmost site (15°N, 38°W) reveal pronounced seasonal cycles of SST, surface heat flux, and MLD during 2000–07 (Fig. 3). SST reaches a maximum in boreal fall and a minimum in the spring. The surface heat flux is in quadrature with SST, tending to heat the mixed layer during boreal spring through fall and tending to cool the mixed layer in boreal winter (Fig. 3c). The MLD varies out of phase with SST, reaching a maximum in March, when SST is at a minimum (Fig. 3d).

SST at 12°N varies in phase with SST at 15°N and is ~1°C higher on average (Fig. 3a). Wind speed undergoes a more pronounced seasonal cycle at 12°N compared to 15°N, tending to enhance the seasonal cycle of LHF at 12°N. The annual mean and seasonal amplitude of absorbed SWR are smaller at 12°N, however, leading to a weaker seasonal cycle of the net surface heat flux at this location in comparison to that at 15°N (Foltz et al. 2003; Fig. 3c). The 8°N, 38°W mooring is located within the latitudinal band of the ITCZ and experiences the highest mean SST of the sites examined in this study (Fig. 3a). The net surface heat flux exhibits a much weaker seasonal cycle at 8°N in comparison to 15° and 12°N owing to weaker seasonal variations of LHF at 8°N. The MLD varies out of phase with SST at 12° and 8°N as at 15°N.

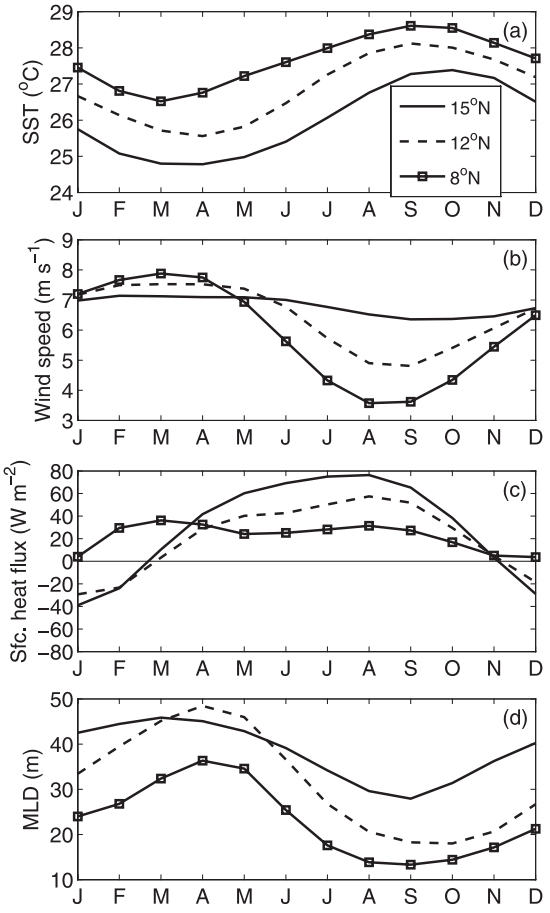

FIG. 3. Seasonal cycles of (a) SST, (b) wind speed, (c) surface heat flux minus penetrative SWR, and (d) mixed layer depth from the PIRATA moorings at 15°N (solid), 12°N (dashed), and 8°N (squares). All time series have been smoothed with a 3-month running mean filter.

We now consider the mixed layer heat balance at 15°N, 38°W in more detail. This location has the longest data record (Fig. 2) and the strongest seasonal cycle of BLT (Figs. 1b,d) of the sites considered in this study. The seasonal cycle of SST at 15°N, 38°W is driven primarily by changes in the net surface heat flux (Foltz et al. 2003; Yu et al. 2006; Fig. 4). Surface shortwave radiation is strongest in boreal spring when the solar zenith angle is high and cloudiness is low. The amount of SWR absorbed by the mixed layer (SWR) also peaks during this season, coinciding with a maximum in mixed layer depth. The magnitude of LHF is greatest in boreal winter when the northeasterly trade winds are strong and the relative humidity is low. Seasonal variations of longwave radiation, sensible heat loss, and horizontal mixed layer heat advection are much weaker in comparison to those of SWR and LHF. As a result, the pronounced decrease in mixed layer heat content and SST during boreal fall and winter is driven primarily by corresponding minima in SWR and LHF, in agreement with the heat budget study of Foltz et al. (2003) at the same mooring location (Figs. 4b,c).

We use the difference between the mixed layer heat storage rate and the sum of the first two terms on the right-hand side of (1) as an estimate of q_{-h}, which we cannot calculate directly. The q_{-h} term includes contributions from entrainment and vertical mixing. The temperature jump at the base of the mixed layer, which affects the magnitude of q_{-h}, is estimated as $\Delta T = T - T_{-h}$ following Moisan and Niiler (1998). Since the base of the mixed layer generally coincides with the top of the thermocline, the temperature of the mixed layer is generally greater than the temperature below. The q_{-h} term undergoes a strong seasonal cycle at 15°N, tending to cool the mixed layer at a rate of up to 80 W m^{-2} during boreal summer and fall and tending to heat the mixed layer by up to 30 W m^{-2} during boreal winter and spring (Fig. 5). The seasonal cycle of q_{-h} varies in phase with the seasonal cycle of ΔT, as would be expected if vertical turbulent processes were driving seasonal variations in q_{-h} (Figs. 5, 6a). The BLT also varies in phase with q_{-h}, reaching a maximum of 15–30 m during boreal winter and spring and a minimum of <5 m in boreal summer and fall (Figs. 5, 6a). The correlation coefficient for monthly climatological BLT and q_{-h} is 0.9 (Table 1).

The strong covariability of ΔT, q_{-h}, and BLT at 15°N suggests that the BLT exerts a significant influence on q_{-h} through its modulation of ΔT. When the barrier layer is thin (<5 m) ΔT is large and positive (the temperature of the mixed layer is greater than the temperature below the mixed layer) and q_{-h} induces cooling at the base of the mixed layer (Figs. 5, 6a). The rapid increase in BLT in boreal fall isolates the base of the mixed layer from the top of the thermocline, resulting in a ΔT that is close to zero. As a result, vertical mixing at the base of the mixed layer does not lead to significant cooling of the mixed layer. Similar effects have been observed and modeled in the western equatorial Pacific and Indian Ocean (e.g., Lukas and Lindstrom 1991; Vialard and Delecluse 1998; Vinayachandran et al. 2002; Du et al. 2005; Masson et al. 2005).

During December–February at 15°N the combination of surface cooling and a thick barrier layer generates a weak temperature inversion at the base of the mixed layer for a period of 1–2 months ($\Delta T < 0$, Fig. 5). During this period q_{-h} tends to heat the mixed layer at a rate of up to 20 W m^{-2} (Fig. 5). Vialard and Delecluse (1998) found similar values of entrainment heating for thick barrier layers (>20 m) in the western tropical Pacific. The 1–2-month period of entrainment warming at 15°N, 38°W does not occur at the same time every year,

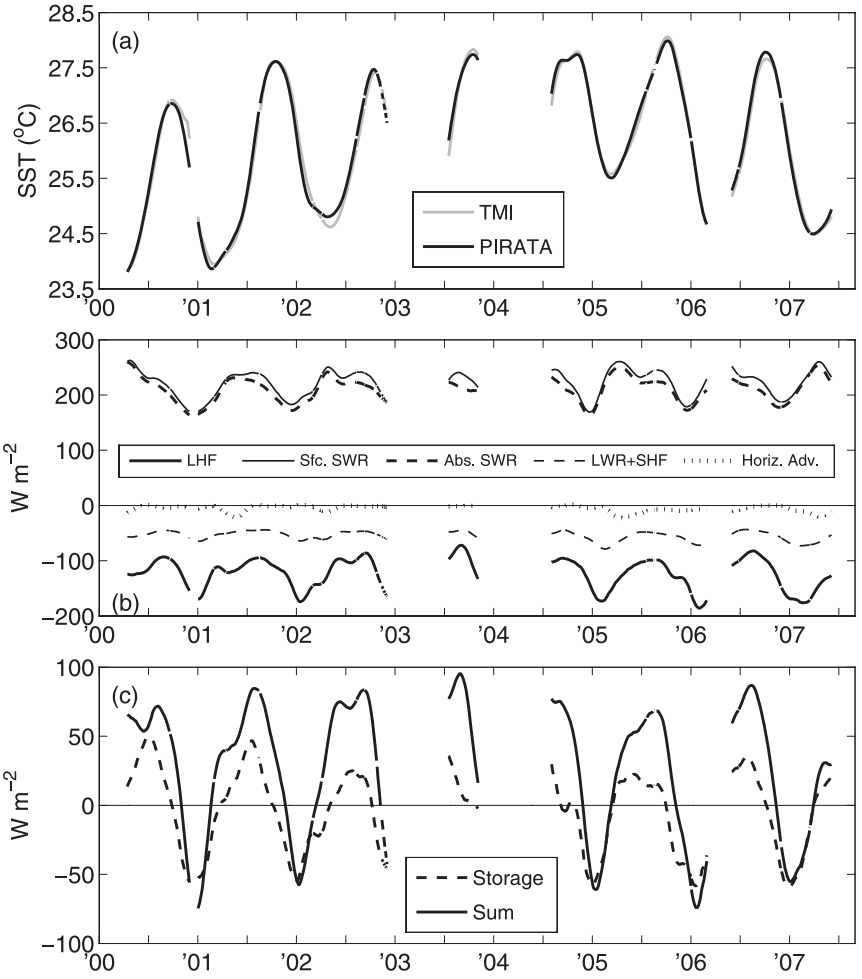

FIG. 4. (a) Daily SST from the PIRATA mooring at 15°N, 38°W (black) and from TMI (gray) at the same location during January 2000–August 2007. (b) Latent heat flux (thick solid), surface SWR (thin solid), SWR absorbed in the mixed layer (thick dashed), sum of net longwave radiation and sensible heat flux (thin dashed), and horizontal advection (dotted) at the same mooring location. (c) Mixed layer heat storage rate (dashed) and sum of the net surface heat flux and horizontal advection (solid). Negative values indicate heat loss from the mixed layer. All time series have been smoothed with consecutive passes of 41- and 61-day running mean filters.

however, so the warming disappears when q_{-h} is averaged to monthly climatological means (Fig. 6a).

Next we consider the 12° and 8°N mooring locations. The BLT at 12°N reaches a maximum of ~15 m in February and a minimum of <5 m in June (Fig. 6b). The seasonal cycle of q_{-h} varies nearly in phase with the seasonal cycle of BLT with a maximum in boreal winter and a minimum in August–October. The correlation between BLT and q_{-h} at 12°N is slightly weaker than at 15°N but is significant at the 10% level (Table 1). The BLT at 8°N reaches a maximum in May–July when precipitation is strong and low-salinity water is transported eastward from the Amazon (Figs. 1c,d). This contrasts sharply with the seasonal cycles of BLT at 15° and 12°N, which exhibit maxima in boreal winter (Fig. 6). Despite the difference in phasing, BLT at 8°N is significantly correlated with q_{-h}, consistent with the BLT$-q_{-h}$ relationships at 15° and 12°N (Table 1).

5. Residual

The BLT and q_{-h} are significantly positively correlated at each mooring location, suggesting that seasonal changes in BLT exert a considerable influence on q_{-h} through their modulation of the vertical turbulent heat flux at the base of the mixed layer. Since q_{-h} is estimated as a residual in the heat balance, it is also likely that uncertainties in the terms we estimated directly

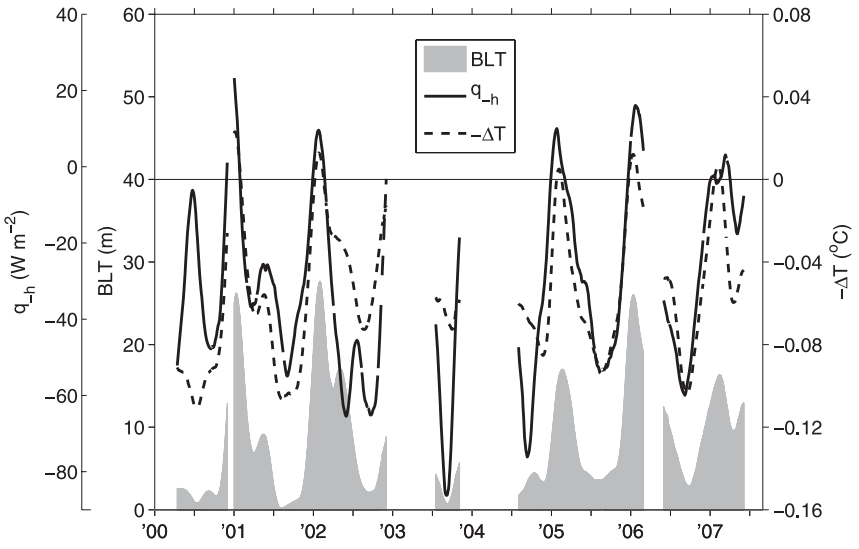

FIG. 5. Difference between T_{-h} and T ($-\Delta$T, solid), barrier layer thickness (shaded), and the heat balance residual (dashed) at 15°N, 38°W. The sign of ΔT has been reversed so that negative values are associated with turbulent cooling and vice versa. All time series have been smoothed with consecutive passes of 41- and 61-day running mean filters.

(i.e., heat storage rate, surface fluxes, and horizontal advection) may introduce noise into our estimates of q_{-h}. In this section we present a detailed analysis of potential errors associated with these terms, expanding on the formal error analysis described in section 3 and presented in Fig. 6.

One significant source of error is mixed layer heat advection since direct estimates of this quantity are not available at the mooring locations. To estimate uncertainties associated with this term we first consider the impact of different mixed layer velocity climatologies on the horizontal advection term. At 15°N the choice of velocity products has a very small impact on the seasonal cycle of advection, with monthly differences generally <5 W m^{-2} (Fig. 7a). At 12°N there is considerably more uncertainty. The OSCAR and GC01 estimates are similar and are both significantly greater than the LG05 estimates during boreal winter (Fig. 7b). The seasonal amplitude of q_{-h} increases when LG05 currents are substituted for GC01 currents at 12°N. It is therefore unlikely that uncertainties in advection can explain the pronounced seasonal cycle of q_{-h} at this location. At 8°N there are significant discrepancies among OSCAR, GC01, and LG05 currents during boreal winter that result in differences in horizontal advection of up to 20 W m^{-2} (Fig. 7c). Substitution of LG05 advection into the heat balance results in a stronger seasonal cycle of q_{-h}, while the use of OSCAR currents results in a significant reduction in the seasonal amplitude of q_{-h}. There are therefore considerable uncertainties in our estimate of the seasonal cycle of q_{-h} at 8°N that are not included in the error estimates shown in Fig. 6c.

TABLE 1. First two columns: amplitudes (defined as the maximum monthly difference) of the seasonal cycles of barrier layer thickness (BLT) and q_{-h}. Third column: correlation between monthly climatological BLT and q_{-h} (bold indicates significance at the 10% level based on a 1000-sample bootstrap test; Wilks 1995).

	BLT amplitude (m)	q_{-h} amplitude (W m^{-2})	Correlation (BLT–q_{-h})
15°N	15	60	**0.9**
12°N	15	50	**0.7**
8°N	10	30	**0.7**

Our estimates of horizontal heat advection are based on monthly climatological currents combined with daily SST gradients and MLD. It is possible that fluctuations of horizontal velocity on time scales shorter than one month may also contribute significantly to the seasonal cycle of mixed layer heat advection. For example, Foltz et al. (2003) suggested that horizontal eddy heat advection tends to cool the mixed layer by up to 30 W m^{-2} during boreal winter and spring along 38°W. Their estimates of eddy heat advection contained a high degree of uncertainty, however, since they were calculated as the residual between dT/dt from drifting buoys and climatological $\partial T/\partial t$ from satellite SST. Here we estimate eddy heat advection using daily measurements of horizontal velocity from the mooring at 15°N available during July 2005–June 2006. Eddy advection is defined as

$$\text{eddy} = \rho c_p h \overline{(\mathbf{v} - \bar{\mathbf{v}}) \cdot (\nabla T - \overline{\nabla T})},$$

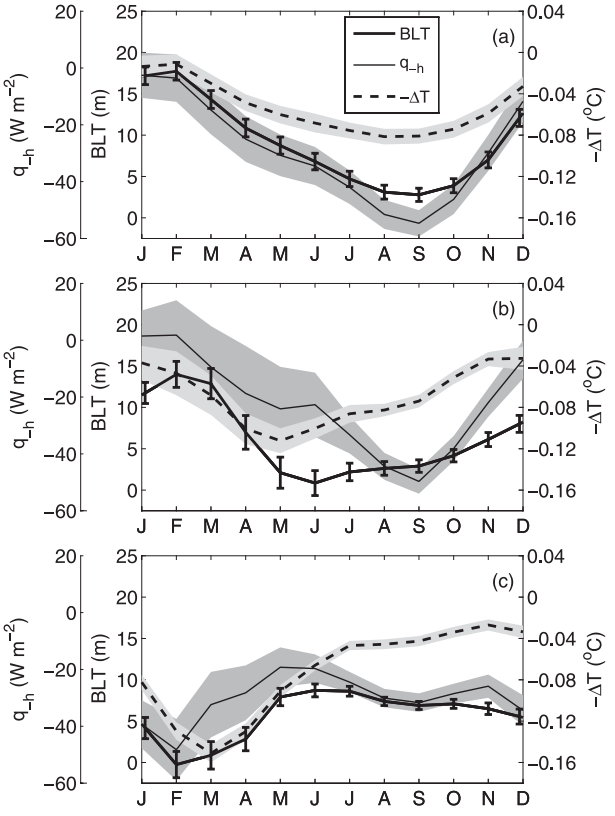

FIG. 6. Seasonal cycles of barrier layer thickness (thick solid line with error bars), heat balance residual (thin solid line with dark shading), and $-\Delta T$ (dashed line with light shading) at (a) 15°N, (b) 12°N, and (c) 8°N. The sign of ΔT has been reversed so that negative values are associated with turbulent cooling and vice versa. Error bars, dark shading, and light shading represent one standard error for BLT, q_{-h}, and $-\Delta T$, respectively. Missing values (February at 8°N for all parameters) were filled with linear interpolation. All time series have been smoothed with a 3-month running mean filter.

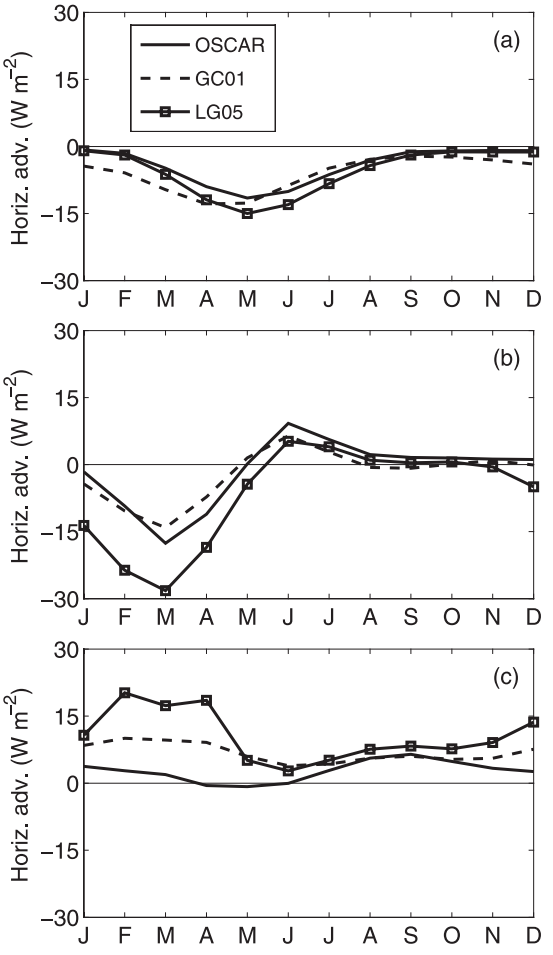

FIG. 7. Horizontal mixed layer heat advection estimated using monthly climatological currents from OSCAR (solid), Grodsky and Carton (2001) (dashed), and Lumpkin and Garzoli (2005) (squares) at (a) 15°N, (b) 12°N, and (c) 8°N. All time series have been smoothed with a 3-month running mean filter.

where $\mathbf{v}$ and h are daily velocity and MLD from the mooring, T is daily TMI SST, and overbars denote monthly means. We find that eddy advection is nearly zero in the annual mean, with a monthly standard deviation of 4 W m^{-2} and no discernable seasonal cycle. The annual mean and standard deviation are small compared to annual mean and seasonal amplitude of q_{-h} at 15°N (-30 ± 30 W m^2, Fig. 6a). It is therefore unlikely that eddy advection contributes significantly to the heat balance at 15°N. It is possible that eddy advection may contribute more significantly at 12° and 8°N. Unlike at 15°N though, we do not have moored velocity measurements at these locations to test this hypothesis.

There are uncertainties in our estimates of SWR that result from the accumulation of dust on the radiometers (e.g., Medovaya et al. 2002; Foltz and McPhaden 2005). These errors are difficult to quantify and are not included in our formal error analyses described in section 3. We have compared the uncorrected SWR measurements to those corrected for dust accumulation, following Foltz and McPhaden (2005), and found monthly climatological differences of ~5–10 W m^{-2} at 15° and 12°N and <5 W m^{-2} at 8°N (with corrected estimates being higher).

It is also possible that seasonal biases in penetrative SWR may contribute significantly to q_{-h}. To estimate the uncertainty associated with this term we have compared our chlorophyll-based estimates of penetrative SWR to those based on a different chlorophyll-based parameterization (Ohlmann 2003). We found differences in the monthly mean seasonal cycles of 10–20 W m^{-2} during boreal summer and fall and 0–10 W m^{-2} during boreal winter and spring [the Ohlmann (2003) algorithm results in more penetrative radiation

in comparison to Morel and Antoine (1994)]. Substitution of absorbed SWR based on Ohlmann (2003) into the heat balance at 15° and 12°N decreases the seasonal amplitude of q_{-h} by 10 W m^{-2} and does not diminish the correlations between BLT and q_{-h}. At 8°N the seasonal amplitude of q_{-h} increases by 10 W m^{-2} when the Ohlmann (2003) algorithm is used, and the correlation between BLT and q_{-h} increases to 0.8. It is therefore unlikely that uncertainties in penetrative SWR can account for the strong covariability between BLT and q_{-h} at the mooring locations.

Uncertainties in our estimates of LWR are likely due primarily to the use of a bulk algorithm to estimate downward longwave radiation instead of direct measurements. Comparison of our LWR estimates, which are based on measurements of air temperature, relative humidity, SWR, and SST from the moorings, to the COADS climatological estimates, reveals differences of ~0–5 W m^{-2} throughout the year at each mooring location (mooring-based LWR emission is lower). These differences are small in comparison to the annual mean and seasonal cycle of q_{-h} at the mooring locations. Comparison of our parameterized LWR estimates to direct measurements of downward LWR from the mooring at 15°N (available during December 2006–August 2007) reveal monthly differences of 10–20 W m^{-2} (direct measurements give more downward LWR and hence less net LWR emission). The differences are greatest during boreal summer. As a result, the amplitude of the seasonal cycle of q_{-h} is increased when the direct measurements of downward LWR are substituted for the parameterized estimates. It is therefore unlikely that uncertainties in LWR can account for the strong seasonal cycle of q_{-h} at 15°N.

Finally, our results are affected by the choice of MLD criterion. To estimate uncertainties associated with this choice, we consider the mixed layer heat balance and BLT at 15°N, 38°W. We choose this location because errors associated with the vertical interpolation of salinity between the sensors at 40 and 120 m is significantly smaller than at 12° and 8°N (based on higher vertical resolution profiles from WOD01). At 15°N the seasonal cycles of q_{-h} and BLT are similar and correlations between them are high (>0.8) for MLD criteria ranging from 0.03–0.15 kg m^{-3}. The main differences occur during boreal winter, when the barrier layer is up to 4 m thinner and q_{-h} decreases by up to 10 W m^{-2} for a 0.15 kg m^{-3} criterion compared to a 0.03 kg m^{-3} criterion.

At 15° and 12°N the magnitudes of the uncertainties described in this section are generally small in comparison to the magnitudes of the seasonal cycles of BLT and q_{-h}, and the correlations between BLT and q_{-h} are not significantly changed for different choices of surface heat flux and mixed layer velocity products. In contrast, at 8°N uncertainties in our estimation of horizontal mixed layer velocity result in large uncertainties in the seasonal cycle of q_{-h}. In the next section we explore the potential impact of the BLT on SST, focusing on the 15° and 12°N mooring locations, where the seasonal cycle of q_{-h} is most robust.

6. Impact of barrier layer thickness on SST

To quantify the effects of the BLT on SST in the central tropical North Atlantic we consider a simple prognostic equation for mixed layer temperature (T) based on (1):

$$T_t = T_{t-1} + \left[\frac{Q_{\text{obs}} + f\Delta q_{-h} + \Delta L}{\rho c_p (h + \Delta h)}\right]_{t-1} \Delta t. \qquad (2)$$

Here Q_{obs} is the observed monthly mean seasonal cycle of total heat flux convergence [rhs of (1)]; Δq_{-h}, ΔL, and Δh are adjustments to the vertical mixing term, LHF, and MLD, respectively; f is a scaling factor ($0 \le f \le 1$); and $\Delta t = 1$ month. When the adjustment terms are zero, (2) returns the actual seasonal cycle of mixed layer temperature. A correction is applied to the LHF to account for changes associated with the deviation of the predicted SST from the observed SST, $\Delta L = L_{\text{pre}} - L_{\text{obs}}$. Here L_{pre} and L_{obs} represent the LHF calculated with the predicted and observed SST, respectively, where the predicted SST is given by (2). In the calculation of ΔL we also adjust air temperature so that the air − sea temperature difference for each month remains constant at its climatological seasonal mean value. Recognizing that factors besides the BLT affect seasonal variations of q_{-h}, we set f equal to the fraction of the seasonal q_{-h} variance explained by BLT (i.e., the squares of the values given in the last column of Table 1).

We have neglected horizontal advection in (2) since we cannot reliably estimate the horizontal distribution of BLT-induced changes in SST. At the 15° and 12°N mooring locations annual mean horizontal advection is at least an order of magnitude smaller than the annual mean value of q_{-h}, and the seasonal amplitude of advection is at least twice as small as the seasonal amplitude of q_{-h}. Based on these scaling arguments, it is unlikely that the inclusion of horizontal advection in (2) would significantly affect the BLT-induced changes in SST presented in this section.

To assess the sensitivity of SST to BLT we first solve (2) setting BLT = 0 and keeping q_{-h} constant at its seasonal minimum value throughout the year (−55 W m^{-2} at 15°N and −50 W m^{-2} at 12°N). Here it is assumed that the deviation of q_{-h} from its minimum value

is primarily related to the presence of a barrier layer. Under this assumption, when BLT is set to zero throughout the year, $\Delta q_{-h} = (q_{-h})_{\min} - q_{-h}$. In this scenario, the MLD is determined only by temperature stratification and the MLD therefore increases by an amount equal to the observed BLT. The rationale for this assumption is that the barrier layer limits vertical mixing to the salt-stratified mixed layer and that, when the barrier layer is removed, the water column mixes down to the base of the isothermal layer.

We find that ignoring the barrier layer results in a cold SST bias after one year (with respect to the observed climatology) of 1.9 ± 0.7°C at 15°N and 1.3 ± 1.2°C at 12°N. Uncertainties in the SST bias at each location were estimated from the accumulation of errors in q_{-h} and h at each time step. The relatively large uncertainty at 12°N compared to 15°N is a consequence of larger uncertainties in q_{-h} at 12°N during boreal winter and spring (Fig. 6). The cold bias at each location results primarily from increases in the magnitude of q_{-h} associated with setting BLT = 0. The Δq_{-h} term in (2) generates a decrease in SST of 4.8°C (4.2°C) at 15°N (12°N), compared to an increase of 0.3°C at both locations due to the Δh term and an increase of 2.6°C at both locations due to ΔL.

The above example provides an estimate of the cold SST bias that develops if the barrier layer is completely ignored at each mooring location. Another interesting case to consider is that in which the annual mean BLT is the same as the observed annual mean BLT, but seasonal variations of BLT are ignored. To estimate the sensitivity of SST to the BLT for this case, we solve (2) with q_{-h} and BLT held constant at their annual mean values (10 m for BLT and -30 W m^{-2} for q_{-h} at 15°N; 5 m and -25 W m^{-2} at 12°N). At both locations the barrier layer is thinnest and cooling associated with q_{-h} is strongest during boreal summer/fall (Fig. 6). As a result, q_{-h} cools the mixed layer more than the annual mean during May–October. Setting q_{-h} equal to its annual mean value therefore generates a maximum warm bias of >1°C during October–November (Fig. 8). There is also a weaker cold bias that peaks during boreal spring. The weaker magnitude of the cold bias with respect to the warm bias is a consequence of two factors. First, the MLD (and thus the heat capacity of the mixed layer) at 15° and 12°N is greatest during boreal winter and spring (Fig. 3d), thus reducing the impact of changes in q_{-h} on SST during these seasons. Second, the BLT reaches a maximum during boreal winter so that the amplitude of the seasonal cycle of MLD increases when BLT is held at its annual mean value. As a result, the heat capacity of the mixed layer is enhanced during boreal winter and diminished during late boreal summer and early fall.

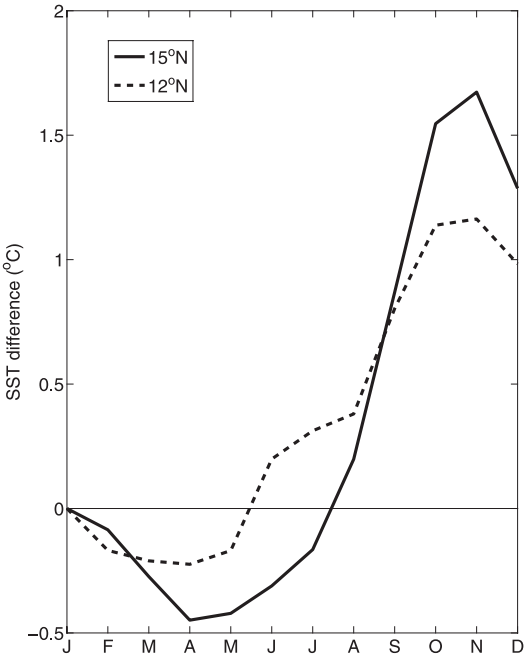

FIG. 8. Deviation of SST from climatology that results if q_{-h} and barrier layer thickness are held at their annual mean values at 15°N (solid) and 12°N (dashed).

The MLD plays an important role in (2) since it affects the sensitivity of SST to changes in surface heat fluxes and q_{-h}. To estimate the impact of changes in the MLD criterion on the predicted SST, (2) is solved at 15°N, 38°W for MLD criteria ranging from 0.03 to 0.15 kg m^{-3}. We find that the SST bias for the first case (setting BLT = 0 throughout the year) is nearly unchanged for this range of MLD criteria since increases in the annual mean MLD are generally compensated for by increases in the magnitude of q_{-h}. For the second case (BLT and q_{-h} set to their annual mean values) using a 0.15 kg m^{-3} criterion instead of a 0.03 kg m^{-3} criterion reduces the seasonal amplitude of the SST bias by about half. The largest reduction occurs in boreal fall when (2) predicts a warm SST bias of 0.8°C for a 0.15 kg m^{-3} criterion versus a warm bias of 1.6°C for a 0.03 kg m^{-3} criterion. For either MLD criterion, the SST bias predicted by (2) is at least one-third of the peak-to-peak amplitude of the seasonal cycle of SST at 15°N, 38°W, suggesting that the seasonal cycle of BLT exerts a significant influence on SST at this location. Higher vertical resolution salinity measurements are needed to assess the impact of changes in MLD criterion at 12°N.

7. Summary and discussion

In this study we examine the impact of barrier layer thickness on SST in the central tropical North Atlantic

Ocean, focusing on three locations where measurements from moored buoys are available (8°, 12°, and 15°N along 38°W). At all three locations it is found that seasonal changes in SST are driven primarily by latent heat flux and shortwave radiation, in agreement with previous studies. The vertical heat flux at the base of the mixed layer (q_{-h}), estimated as a residual in the heat balance, also undergoes a pronounced seasonal cycle at each location. The seasonal cycle of q_{-h} is significantly positively correlated with the seasonal cycle of barrier layer thickness (i.e., cooling from turbulent mixing is weakest when the barrier layer is thickest), suggesting that seasonal changes in the barrier layer thickness (BLT) exert a significant influence on q_{-h} through their modulation of the vertical temperature gradient at the base of the mixed layer (ΔT). The impact of the barrier layer on ΔT and q_{-h} is strongest at 15°N, 38°W where the seasonal cycle of BLT is strongest. The combination of a thick barrier layer and strong surface cooling during boreal winter of some years at this location is associated with a reversal in the sign of ΔT and a 1–2-month period of entrainment warming.

Using a simple mixed layer model we showed that, if seasonal variations of BLT are ignored, cold SST biases of ~1–1.5°C develop within a year at 15° and 12°N. These biases are about one-half the magnitude to the climatological seasonal cycle of SST in the central tropical North Atlantic, suggesting that forced ocean and coupled ocean–atmosphere models that do not properly simulate the barrier layer may have difficulty reproducing the seasonal cycle of SST in the tropical North Atlantic.

The seasonal mixed layer heat budgets presented in this study generally agree with those of Foltz et al. (2003), which are based on measurements from the same PIRATA moorings. At all three mooring locations seasonal changes in mixed layer content are balanced primarily by latent heat loss and shortwave radiation. During May–December at 15°N, 38°W and June–October at 12°N, 38°W Foltz et al. found a missing source of cooling to the mixed layer of up to 50 W m^{-2} that they attributed partially to vertical turbulent mixing at the base of the mixed layer. We also find a missing source of cooling at these locations during these months. During the remainder of the year (January–April at 15°N and November–May at 12°N), Foltz et al. found a missing source of warming to the mixed layer of up to 40 W m^{-2}, whereas we found a missing source of cooling. The discrepancies are due mainly to differences in the estimation of horizontal eddy heat advection and penetrative shortwave radiation. In this study we estimated eddy advection using direct velocity measurements from the mooring at 15°N, 38°W and found that it contributes insignificantly in comparison to the other terms in the heat balance. In contrast, Foltz et al. (2003) estimated eddy advection using SST from surface drifters and monthly climatological SST and found that it cools the mixed layer during January–April at 15° and 12°N. The differences in penetrative shortwave radiation are due to the use of different models. In the present study we estimate penetrative radiation from a model that depends on chlorophyll-*a* concentration. This model results in ~15 W m^{-2} less penetrative radiation than the constant *e*-folding depth model used by Foltz et al. (2003). The chlorophyll-based algorithm is better in principle since it accounts for changes in the optical transparency of the mixed layer associated with changes in biological productivity.

At 15°N, 38°W we find that q_{-h} averages -10 W m^{-2} when BLT $>$ 10 m and -40 W m^{-2} when BLT $<$ 10 m based on monthly mean data that includes interannual variability. Results are similar when monthly mean climatologies of BLT and q_{-h} are used in the calculation. The impact of BLT on q_{-h} is weaker at 12° and 8°N in comparison to 15°N ($q_{-h} = 0$ W m^{-2} for BLT $>$ 10 m and -30 W m^{-2} for BLT $<$ 10 m at 12°N; $q_{-h} = -20$ W m^{-2} for BLT $>$ 10 m and -30 W m^{-2} for BLT $<$ 10 m at 8°N).

The decrease in entrainment cooling with increasing BLT that we found in the central tropical North Atlantic is consistent with the results of Vialard and Delecluse (1998) in the western equatorial Pacific, though we found a slightly larger sensitivity of q_{-h} to BLT in the Atlantic. Close to the equator (2°S–2°N, 170°E–180°) Vialard and Delecluse found that $q_{-h} \sim 0$ for 10 m $<$ BLT $<$ 20 m and $q_{-h} \sim -20$ W m^{-2} for BLT $<$ 10 m based on 5-day averages from a numerical model simulation during 1985–94. For a broader latitude range (10°S–10°N, 140°E–180°) the effect was much weaker (differences in q_{-h} of ~5 W m^{-2}). They attributed the greater sensitivity near the equator to enhanced velocity shear near the base of the mixed layer.

The greater sensitivity of q_{-h} to BLT in the central tropical North Atlantic in comparison to the western equatorial Pacific likely results from a combination of factors, including differences in surface buoyancy and wind stress forcing and differences in barrier layer formation mechanisms. For example, in the western equatorial Pacific precipitation and the subduction of high salinity water from the central equatorial Pacific both appear to contribute significantly to barrier layer formation. In contrast, in the tropical North Atlantic precipitation is much weaker, whereas southward advection of high salinity subtropical water beneath northward advection of low salinity water from the ITCZ is important. These differences may in turn affect stratification and vertical mixing rates in the two basins.

The impact of BLT on SST in the central tropical North Atlantic that is found in this study is generally consistent with previous modeling studies in the Pacific and Indian Oceans. In the western equatorial Pacific Vialard and Delecluse (1998) found a cold bias of ~0.5°C after one year when salinity effects were ignored in their model. Similarly, Masson et al. (2005) found a maximum difference of 0.5°C in the southeastern Arabian Sea that peaked two months after the seasonal maximum in BLT. These values are lower than the 1°–2°C biases we found in the tropical North Atlantic when barrier layer effects are ignored. The differences can likely be attributed to a combination of differences in mixed layer depth, the sensitivity of vertical mixing to BLT, and to the different models used. Vialard and Delecluse (1998) and Masson et al. (2005) used ocean general circulation models and estimated barrier layer effects by suppressing the contribution of salinity to vertical mixing. In contrast, in this study we used a much simpler model based on observed surface heat fluxes, MLD, and BLT. Our model may overestimate the effects of the BLT on SST since it artificially prescribes constant barrier layer thicknesses for sensitivity tests and ignores the redistribution of SST anomalies by horizontal currents. On the other hand, results from numerical models may be biased owing to errors in surface buoyancy and wind stress forcing and parameterizations of vertical mixing.

The results of this study indicate that changes in barrier layer thickness contribute significantly to the seasonal cycle of SST in the central tropical North Atlantic through their modulation of the vertical mixing of heat at the base of the mixed layer. Nevertheless, there are uncertainties in our estimates of the mixed layer heat budget that are related to the coarse vertical resolution of salinity on the moorings, combined with uncertainties in surface flux estimates and a lack of high temporal resolution horizontal velocity measurements. A better understanding of the seasonal mixed layer heat budget and the impact of barrier layer thickness on SST will depend on continued in situ measurements from PIRATA, Argo, and surface-drifting buoys, in combination with well-designed numerical modeling experiments.

Acknowledgments. We thank three anonymous reviewers for their helpful suggestions. This research was supported by NOAA's Climate Program Office.

REFERENCES

Blanke, B., M. Arhan, A. Lazar, and G. Prevost, 2002: A Lagrangian numerical investigation of the origins and fates of the salinity maximum water in the Atlantic. *J. Geophys. Res.,* **107,** 3163, doi:10.1029/2002JC001318.

Bonjean, F., and G. S. E. Lagerloef, 2002: Diagnostic model and analysis of the surface currents in the tropical Pacific Ocean. *J. Phys. Oceanogr.,* **32,** 2938–2954.

Breugem, W.-P., P. Chang, C. J. Jang, J. Mignot, and W. Hazeleger, 2008: Barrier layers and tropical Atlantic SST biases in coupled GCMs. *Tellus,* **60A,** 885–897.

Carton, J. A., and Z. X. Zhou, 1997: Annual cycle of sea surface temperature in the tropical Atlantic Ocean. *J. Geophys. Res.,* **102,** 27 813–27 824.

——, G. Chepurin, X. H. Cao, and B. Giese, 2000: A simple ocean data assimilation analysis of the global upper ocean 1950–95. Part I: Methodology. *J. Phys. Oceanogr.,* **30,** 294–309.

Clark, N.E., L. Eber, R.M. Laurs, J.A. Renner, and J.F.T. Saur, 1974: Heat exchange between ocean and atmosphere in the eastern North Pacific for 1961–71. NOAA Tech. Rep. NMRS SSRF-682, 108 pp.

Cronin, M. F., and M. J. McPhaden, 1997: The upper ocean heat balance in the western equatorial Pacific warm pool during September–December 1992. *J. Geophys. Res.,* **102,** 8533–8553.

da Silva, A., A. C. Young-Molling, and S. Levitus, 1994: *Algorithms and Procedures. Vol. 1, Atlas of Surface Marine Data 1994*, NOAA Atlas NESDIS 6, 83 pp.

Davis, R. E., 1976: Predictability of sea surface temperatures and sea level pressure anomalies over the North Pacific Ocean. *J. Phys. Oceanogr.,* **6,** 249–266.

de Boyer Montégut, C., J. Mignot, A. Lazar, and S. Cravatte, 2007: Control of salinity on the mixed layer depth in the world ocean. Part I: General description. *J. Geophys. Res.,* **112,** C06011, doi:10.1029/2006JC003953.

De Witt, D. G., and E. K. Schneider, 1999: The processes determining the annual cycle of equatorial sea surface temperature: A coupled general circulation model perspective. *Mon. Wea. Rev.,* **127,** 381–395.

Du, Y., T. D. Qu, G. Meyers, Y. Masumoto, and H. Sasaki, 2005: Seasonal heat budget in the mixed layer of the southeastern tropical Indian Ocean in a high-resolution ocean general circulation model. *J. Geophys. Res.,* **110,** C04012, doi:10.1029/2004JC002845.

Fairall, C. W., E. F. Bradley, D. P. Rogers, J. B. Edson, and G. S. Young, 1996: Bulk parameterization of air-sea fluxes for Tropical Ocean-Global Atmosphere Coupled Ocean-Atmosphere Response Experiment. *J. Geophys. Res.,* **101,** 3747–3764.

——, ——, J. E. Hare, A. A. Grachev, and J. B. Edson, 2003: Bulk parameterization of air–sea fluxes: Updates and verification for the COARE algorithm. *J. Climate,* **16,** 571–591.

Folland, C. K., T. N. Palmer, and D. E. Parker, 1986: Sahel rainfall and worldwide sea temperatures, 1901–85. *Nature,* **320,** 602–607.

Foltz, G. R., and M. J. McPhaden, 2005: Mixed layer heat balance on intraseasonal time scales in the northwestern tropical Atlantic Ocean. *J. Climate,* **18,** 4168–4184.

——, and ——, 2008: Seasonal mixed layer salinity balance of the tropical North Atlantic Ocean. *J. Geophys. Res.,* **113,** C02013, doi:10.1029/2007JC004178.

——, S. A. Grodsky, J. A. Carton, and M. J. McPhaden, 2003: Seasonal mixed layer heat budget of the tropical Atlantic Ocean. *J. Geophys. Res.,* **108,** 3146, doi:10.1029/2002JC001584.

——, ——, ——, and ——, 2004: Seasonal salt budget of the northwestern tropical Atlantic Ocean along 38°W. *J. Geophys. Res.,* **109,** C03052, doi:10.1029/2003JC002111.

Giannini, A., R. Saravanan, and P. Chang, 2003: Oceanic forcing of Sahel rainfall on interannual to interdecadal time scales. *Science,* **302,** 1027–1030.

Goldenberg, S. B., C. W. Landsea, A. M. Mestaz-Nunez, and W. M. Gray, 2001: The recent increase in Atlantic hurricane activity: Causes and implications. *Science,* **293,** 474–479.

Grodsky, S. A., and J. A. Carton, 2001: Intense surface currents in the tropical Pacific during 1996–1998. *J. Geophys. Res.,* **106,** 16 673–16 684.

Hastenrath, S., 1984: Interannual variability and annual cycle—Mechanisms of circulation and climate in the tropical Atlantic sector. *Mon. Wea. Rev.,* **112,** 1097–1107.

——, and L. Greischar, 1993: Circulation mechanisms related to Northeast Brazil rainfall anomalies. *J. Geophys. Res.,* **98,** 5093–5102.

Jiang, C., M. F. Cronin, K. A. Kelly, and L. Thompson, 2005: Evaluation of a hybrid satellite- and NWP-based turbulent heat flux product using Tropical Atmosphere-Ocean (TAO) buoys. *J. Geophys. Res.,* **110,** C09007, doi:10.1029/2004JC002824.

Kanamitsu, M., W. Ebisuzaki, J. Woollen, S. K. Yang, J. J. Hnilo, M. Fiorino, and G. L. Potter, 2002: NCEP–DOE AMIP-II Reanalysis (R-2). *Bull. Amer. Meteor. Soc.,* **83,** 1631–1643.

Kossin, J. P., and D. J. Vimont, 2007: A more general framework for understanding Atlantic hurricane variability and trends. *Bull. Amer. Meteor. Soc.,* **88,** 1767–1781.

Lukas, R., and E. Lindstrom, 1991: The mixed layer of the western equatorial Pacific Ocean. *J. Geophys. Res.,* **96,** (Suppl.), 3343–3357.

Lumpkin, R., and S. L. Garzoli, 2005: Near-surface circulation in the tropical Atlantic Ocean. *Deep-Sea Res. I,* **52,** 495–518.

Maes, C., J. Picaut, and S. Belamari, 2002: Salinity barrier layer and onset of El Niño in a Pacific coupled model. *Geophys. Res. Lett.,* **29,** 2206, doi:10.1029/2002GL016029.

Masson, S., and P. Delecluse, 2001: Influence of the Amazon river runoff on the tropical Atlantic. *Phys. Chem. Earth,* **26,** 137–142.

——, and Coauthors, 2005: Impact of barrier layer on winter-spring variability of the southeastern Arabian Sea. *Geophys. Res. Lett.,* **32,** L07703, doi:10.1029/2004GL021980.

Medovaya, M. D., D. E. Waliser, R. A. Weller, and M. J. McPhaden, 2002: Assessing ocean buoy shortwave observations using clear-sky model calculations. *J. Geophys. Res.,* **107,** 3014, doi:10.1029/2000JC000558.

Mignot, J., C. de Boyer Montégut, A. Lazar, and S. Cravatte, 2007: Control of salinity on the mixed layer depth in the world ocean: 2. Tropical areas. *J. Geophys. Res.,* **112,** C10010, doi:10.1029/2006JC003954.

Mitchell, T. P., and J. M. Wallace, 1992: The annual cycle in equatorial convection and sea surface temperature. *J. Climate,* **5,** 1140–1156.

Moisan, J. R., and P. P. Niiler, 1998: The seasonal heat budget of the North Pacific: Net heat flux and heat storage rates (1950–1990). *J. Phys. Oceanogr.,* **28,** 401–421.

Monterey, G. I., and S. Levitus, 1997: *Seasonal Variability of Mixed Layer Depth for the World Ocean*. NOAA Atlas NESDIS 14, 96 pp.

Morel, A., and D. Antoine, 1994: Heating rate within the upper ocean in relation to its bio-optical state. *J. Phys. Oceanogr.,* **24,** 1652–1665.

Muller-Karger, F. E., C. R. McClain, and P. L. Richardson, 1988: The dispersal of the Amazon's water. *Nature,* **333,** 56–58.

Nobre, C., and J. Shukla, 1996: Variations of sea surface temperature, wind stress, and rainfall over the tropical Atlantic and South America. *J. Climate,* **9,** 2464–2479.

Ohlmann, J. C., 2003: Ocean radiant heating in climate models. *J. Climate,* **16,** 1337–1351.

Okajima, H., S. P. Xie, and A. Numaguti, 2003: Interhemispheric coherence of tropical climate variability: Effect of the climatological ITCZ. *J. Meteor. Soc. Japan,* **81,** 1371–1386.

Pailler, K., B. Bourles, and Y. Gouriou, 1999: The barrier layer in the western tropical Atlantic Ocean. *Geophys. Res. Lett.,* **26,** 2069–2072.

Sato, K., T. Suga, and K. Hanawa, 2006: Barrier layers in the subtropical gyres of the world's oceans. *Geophys. Res. Lett.,* **33,** L08603, doi:10.1029/2005GL025631.

Saunders, M. A., and A. S. Lea, 2008: Large contribution of sea surface warming to recent increase in Atlantic hurricane activity. *Nature,* **451,** 557–560.

Servain, J., A. J. Busalacchi, M. J. McPhaden, A. D. Moura, G. Reverdin, M. Vianna, and S. E. Zebiak, 1998: A Pilot Research Moored Array in the Tropical Atlantic (PIRATA). *Bull. Amer. Meteor. Soc.,* **79,** 2019–2031.

Shapiro, L. J., and S. B. Goldenberg, 1998: Atlantic sea surface temperatures and tropical cyclone formation. *J. Climate,* **11,** 578–590.

Sprintall, J., and M. Tomczak, 1992: Evidence of the barrier layer in the surface layer of the tropics. *J. Geophys. Res.,* **97,** 7305–7316.

Sweeney, C., A. Gnanadesikan, S. M. Griffies, M. J. Harrison, A. J. Rosati, and B. L. Samuels, 2005: Impacts of shortwave penetration depth on large-scale ocean circulation and heat transport. *J. Phys. Oceanogr.,* **35,** 1103–1119.

Swenson, M. S., and D. V. Hansen, 1999: Tropical Pacific Ocean mixed layer heat budget: The Pacific cold tongue. *J. Phys. Oceanogr.,* **29,** 69–81.

Vialard, J., and P. Delecluse, 1998: An OGCM study for the TOGA decade. Part I: Role of salinity in the physics of the western Pacific fresh pool. *J. Phys. Oceanogr.,* **28,** 1071–1088.

Vinayachandran, P. N., V. S. N. Murty, and V. Ramesh Babu, 2002: Observations of barrier layer formation in the Bay of Bengal during summer monsoon. *J. Geophys. Res.,* **107,** 8018, doi:10.1029/2001JC000831.

Wang, C. Z., D. B. Enfield, S. K. Lee, and C. W. Landsea, 2006: Influences of the Atlantic warm pool on western hemisphere summer rainfall and Atlantic hurricanes. *J. Climate,* **19,** 3011–3028.

Wilks, D. S., 1995: *Statistical Methods in the Atmospheric Sciences*. Academic Press, 467 pp.

Yu, L. S., X. Z. Jin, and R. A. Weller, 2006: Role of net surface heat flux in seasonal variations of sea surface temperature in the tropical Atlantic Ocean. *J. Climate,* **19,** 6153–6169.